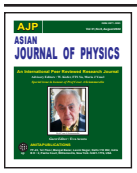

Asian Journal of Physics
Vol. 31, No 8 (2022) 847-862
Available on: www.asianjournalofphysics.com

ap

Hole-drilling method combined with DSPI: challenges and achievements for residual stress measurements

Matias Roberto Viotti, Filipe Zanini Broetto and Armando Albertazzi (Jr)

Laboratório de Metrologia e Automatização (*Labmetro*),

Universidade Federal de Santa Catarina, Florianópolis, SC, Brazil.

This article is dedicated to Professor Cesar Sciammarella

The hole drilling technique is extensively applied to measure residual stresses in mechanical components and can be applied both in laboratory and industrial environments. Usually, the hole drilling method is combined with electrical strain gages. Many research group activities have been oriented to replace the measurement with strain gages by optical techniques. These techniques are appropriate for rapid measurements considering they are non-contacting methods, and they are suitable to perform full-field evaluation. One limitation for the hole drilling technique is its depth sensitivity. Typically, the method can only identify stresses up to a depth of approximately the radius of the hole. Consequently, for a conventional hole diameter of 1.6 mm, the hole depth will be between 0.8 mm and 1 mm. This paper shows the achievements of Labmetro during the last decade regarding the application of radial in-plane speckle interferometer to the measurement of residual stresses in real situations involving the oil and gas industry. Additionally, the paper also shows the advancements that have made possible to achieve higher depths. The examples presented in the paper clearly show the suitability of the speckle metrology as a supplementary tool for the assessment of the integrity in structures.

Keywords: Hole-drilling, Speckle interferometry, Radial sensitivity, Residual stresses.

1 Introduction

In the modern world, a large variety of engineering components are currently used in the industry or people's life to solve practical problems and to bring comfort. These components and systems are either designed as a solution to an existing engineering problem or as part of entirely new products. The design task is executed by multidisciplinary groups of designers, researchers, engineers, technicians and so on. The resulting product must be functional, safe, reliable, manufacturable, competitive, and marketable [1].

A set of parameters are usually analyzed during the definition of the problem, data is gathered and analyzed to find the most appropriate solution. One of the most important features to be considered in practical applications is the structural integrity and reliability of the component during its product life cycle (PLC) i.e, its capability to withstand service loads, effectively and efficiently, without failure [2].

The stress field presented within some materials without the application of external loads, or other stress sources, is known as residual stress field [3]. These stresses combine with stresses introduced by the applied loads and, depending on their level and direction, can either be beneficial or detrimental to the performance and life-time of the components. Therefore, it is important to truthfully measure such stresses during the design/manufacturing process and include them in the integrity analysis. Such analysis must also include safety coefficients, working conditions considering temperature and pressure, service loads, and other

Corresponding author
e mail: matiasviotti@gmail.com (Matias Roberto Viotti)

parameters, that are used to feed a suitable mathematical model which represents the component/system as close to realty as possible.

The hole drilling technique is one of the most widespread techniques for measuring residual stresses [4,5]. This technique consists of removing stressed material from the region of interest, and then measuring the displacement or strain field in the surrounding area. The material is removed in the drilling process by a cutting tool, usually an end mill, and since the material removed contained stresses, the remaining material surrounding the hole must rearrange to reach new equilibrium. Given the physical characteristics of the process, there is a limitation that prevents stresses released at higher depths to cause a measurable effect on the surface. For a typical 1.6 mm hole diameter, the maximum depth that stresses can be measured is around 0.8 mm to 1 mm.

Traditionally, the hole drilling method has been applied for uniform stress determination. Nevertheless, real applications usually involve residual stresses considered as nonuniform. In other words, the stress levels vary along the hole depth. The literature presents many works associated to the development of a method to compute this kind of stresses by utilizing the set of strains which are released during the hole increments. The solution proposed is in the form of an inverse problem known as the integral method. [3,6,7]. The recent version of the ASTM E837 standard takes into account this solution for non-uniform residual stresses [3].

The mathematical formulation to compute residual stresses from the strain/displacement field around the hole is typically an inverse problem [3,6,7]. The integral method is usually applied for the hole drilling method combined with strain gages. The solution for the computation of the stresses uses a set of matrices which are numerically ill conditioned [7,15]. Consequently, inaccuracies in the measured strains/displacements are magnified in the stress solution. Results are usually less sensitive to these errors in the first hole increments, where the signal is stronger, but more sensitive for the last step of the hole, which limits the depth achieved by this technique. Ref [7] presented an effective methodology to deal with strain errors for hole depths equivalent to the hole radius.

Despite of strains being usually monitored with specialized three-element strain gage rosettes, the combination of the hole drilling technique with strain gage sensors presents some practical and economical drawbacks such as: (a) time consuming installation , (b) need of careful surface preparation and (c) significant error sensitivity to strain gage misalignments [4,8,9]. Due to these disadvantages, several optical techniques have been developed during the last decades to replace strain gage measurements [10]. Digital Speckle Pattern Interferometry (DSPI) is identified as an appropriate optical method due to its high sensitivity, non contacting and fast image processing. These features confer high suitability for industrial inspection.

In order to measure in-plane residual stress fields with unknown principal direction, DSPI systems based on two sets of dual-beam illumination arrangements can be used to determine separately both orthogonal stress components [11]. In the case of the interferometer developed by Moore and Tyrer [11], the two in-plane measurements are taken simultaneously using different polarization in each illumination set. Thus, each in-plane set has two orthogonal beams with a kind of polarization which avoids the interference between them. However, optically rough surfaces frequently depolarize both beams. Thus, cross interference happens frequently. A step forward to solve these problems was given by Albertazzi *et al*, from the Labmetro team, with the development of a novel double illumination DSPI system to measure radial in-plane displacement fields [12]. The application of a conical mirror in the system presented in Ref [12] presents a set of practical restrictions which limit its employment for laboratory purposes. A diffractive optical element (DOE) with axis-symmetrical and binary structures was developed and used as an alternative to the conical mirror system. The DOE is used as a beam-splitting grating to generate the double illumination pattern [13]. This DOE was mounted in a measurement module which was combined with a holed-drilling module. This modular arrangement used a universal base to interchange modules during the measurement by means of a precision

mechanism composed by magnetic devices and kinematic principles. In order to apply the standardized procedure for a non-uniform stress measurement, both measurement and drilling modules are usually switched 20 times. The measurement becomes an exhausting task, and the number of variables affecting the results is increased considerably. Thus, a more advanced system was developed to be more compact, robust and more user friendly [14]. This device consisted of an universal base supporting the hole-drilling and measurement modules. A rotational mechanism allowed a high precision, quick and simple exchanging. A set of the last achievements obtained at Labmetro with this device will be shown in this paper. Additionally, challenges posed for future applications will be cited.

The use of radial in-plane interferometer makes it easier to adapt different end mills without much extra effort, thus giving some flexibility to increase the sensitivity at higher depths. For example, a 3mm end mill could be used in the proposed modular device to measure stresses with high confidence up to 2mm. This paper shows this modified system based on the radial in-plane interferometer presented earlier. The formalism presented in Ref 15 is applied for the computation of the residual stresses considering the displacement field measured for the interferometer. A few real application cases are discussed and then some experimental results are also shown. Additionally, challenges for future applications are also cited along the text.

2 Residual stress determination with DSPI

2.1 Hole drilling-DSPI combined device principles

A specific diffractive optical component (DOE) with axis-symmetrical structures is used to achieve sensitivity to in-plane displacements. Figure 1 (a) shows schematics of a cross-section of the DOE. It is a disk constructed by a set of concentric grooves with a fix period p of about 1 μm and a circular area in the center without structures. The DOE is positioned close to the surface under evaluation. The DOE is illuminated with collimated laser light illuminated. Figure 1 (a) additionally presents four specifically selected light rays diffracted by the order identified as – 1 (dashed lines) and the order + 1 (represented by solid lines). The DOE is designed so that the zero order is canceled out. Considering only the first order from each side, the region in the center on the sample receives double illumination. Taking into account a point P, the diffracted rays symmetrically illuminate the point P along the plane of incidence which contains the incidence vectors $\mathbf{k_1}$ and $\mathbf{k_2}$. The sensitivity vector $\mathbf{k}$ is obtained from the subtraction of $\mathbf{k_1}$ and $\mathbf{k_2}$. If the incidence angles are symmetrical with respect to the DOE axis, then the vector $\mathbf{k}$ is parallel to the surface of the sample and point P has in-plane sensitivity.

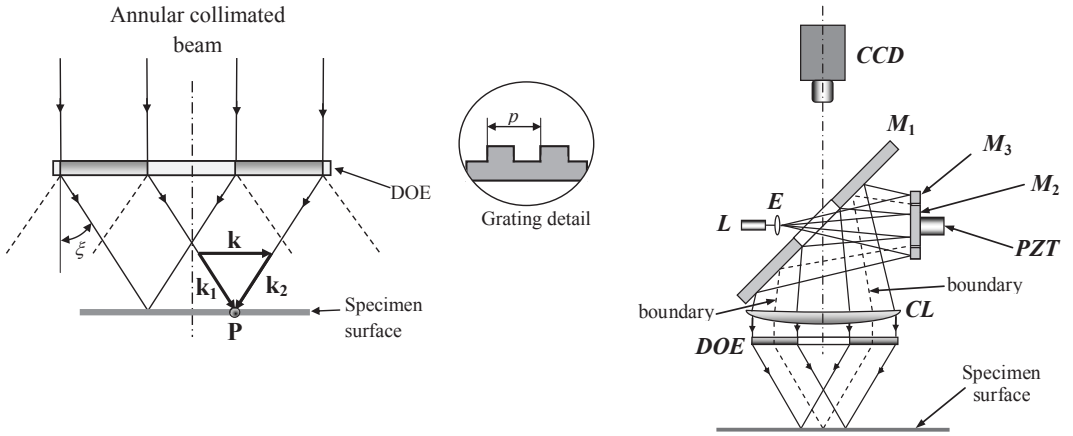

(a) (b)

Fig 1. (a) Cross-section of the DOE showing the first diffraction orders. (b) Optical arrangement of a radial in-plane interferometer.

The cross section of Fig 1 (a) can be extended circumferentially to the whole DOE. Thus, every point on the specimen surface receives light from a single pair of light rays and the entire illuminated circular region has in-plane radial sensitivity. The only exception is the center of the circular region that is a singular point. A more detailed description about radial in-plane sensitivity can be found in Refs [13 and 16].

Figure 1(b) shows the practical configuration used to build a compact device based on the DOE arrangement [13,16]. The light coming from a diode laser (L) is expanded with the lens (E). Next, it goes through the elliptical hole in the mirror M_1. This mirror has a 45º angle with the axis of the DOE. The expanded beam impinges on mirrors M_2 and M_3. After that, it is reflected back to the mirror M_1. After this reflection, the beam is collimated by lens (CL) to form an annular collimated beam. As final step, the DOE diffracts the light in the 1st diffraction order directing it to the central region on the specimen surface. The elliptical hole in mirror M_1 is designed to avoid triple illumination in the illuminated region on the sample. Additionally, it is a viewing window for the CCD camera to image the surface under measurement. The illuminated region has a diameter of approximately 10 mm.

The system composed by mirrors M_2 and M_3 presents the feature that they are concentric circular mirrors. Mirror M_2 is attached to a piezoelectric actuator (PZT). On the other hand, M_3 has a central hole with a slightly larger diameter than the external diameter of M_2. Figure 1 (b) shows the boundary between both beams as dashed lines. As M_3 is fixed, the translation of M_2 by the PZT along its axial direction introduces a relative phase difference between both reflected beams. The boundary region between them is indicated with dashed lines in Fig 2. In accordance with this figure, it can be noted that every illuminated superficial point has only one ray coming each from M_2 and from M_3. Consequently, the piezoelectric actuator permits the application of a uniform phase shift for the whole illuminated circular area to determine the optical phase distribution by specific phase shifting algorithms.

Due to the axisymmetric nature, the light intensity over the whole circular illuminated area is not constant on the sample surface. Moreover, it is especially higher at the central point due to the cumulative light contribution from all cross-sections. As a result, a bright spot is noticed at the center and the interference contrast is reduced. To overcome this problem, the outer diameter of M_2 and inner diameter of M_3 are deliberately chosen so that there is a gap of about 0.5 mm at the position where rays would be reflected.

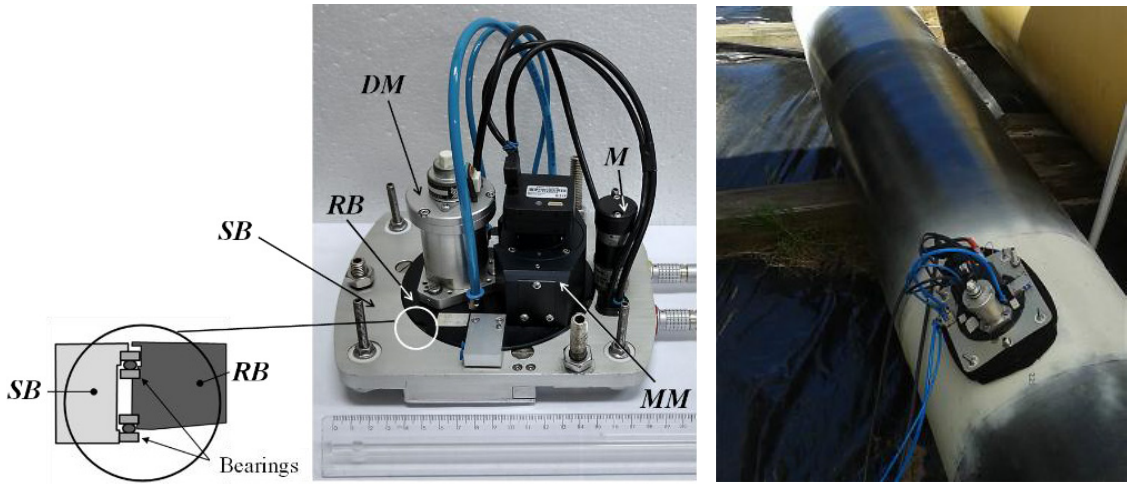

(a) (b)

Fig 2. DSPI portable device: (a) compact device details and (b) application case.

Figure 2(a) shows the DSPI apparatus with the modular configuration. It involves two principal modules: the hole drilling module (DM) and the measurement module (*MM*). In the photographs, they are fixed to a rotational base (RB) and mounted on a supporting base (*SB*). In addition, a DC motor (*M*) is employed to automatically rotate *RB*. Two thin section ball bearings are set between *SB* and *RB* making available a quick and friendly module interchanging (please see the inset with the cross-section). This configuration allows rotation with high accuracy and smooth movement. Finally, kinematic mechanisms permit the correct module positioning during the acquisition and drilling operations. The combination of high precision bearings and kinematic mechanisms limits positioning errors to less than $\lambda/2$.

A successful residual stress measurement using the system mentioned here is achieved by following an experimental procedure. First, the portable device in Fig 2 (a) is placed on top of the sample with the MM aligned with measurement point. The supporting base is rigidly clamped by three sharp feet and four regulating strong magnetic legs. Next, the measurement module (MM) is employed to acquire a set of phase-shifted speckle interferograms to calculate the reference phase distribution. After that, the hole drilling module (DM) is automatically rotated into position by the rotating base (RB) to perform the first drilling step. The first hole increment is machined to a depth of ~0.05 mm. After the repositioning of the measurement module (MM), a second set of phase-shifted speckle interferograms is acquired and a new phase distribution is achieved and stored for next computations. As a real application, Fig 2 (b) shows the portable device performing measurement. This procedure is repeated for each hole increment till the final depth is achieved. As a result, a set of wraped and continues phase maps are obtained and their associated displacements fields are determined.

2.2 Hole drilling-DSPI model for residual stress

When a hole is drilled into a material with residual stresses, they are released due to changes in the local equilibrium state of stress. The resultant displacement field generated in the neighborhood of the hole can be measured with electrical strain gages or with optical methods. The ASTM standard E837 [5] defines the methodology used to compute the stresses from the measured strains. For the case involving optical methods, Ref [15] presents a formalism developed specially for the computation by different optical techniques as well as for Cartesian or polar optical layouts.

For the uniform in-plane residual stresses σ_x, σ_y, σ_z, the released surface in-plane radial displacement D_r is [15].

$$\frac{1}{a} D_r(r,\theta) = \frac{1+\upsilon}{E} P u_r(r) + \frac{1}{E} Q \upsilon_r(r) \cos 2\theta + \frac{1}{E} T \upsilon_r(r) \sin 2\theta \tag{1}$$

where

$$P = (\sigma_x + \sigma_y)/2,\ Q = (\sigma_x - \sigma_y)/2,\ T = \tau_{xy} \tag{2}$$

where u_r and υ_r are the radial distributions of radial displacement, respectively associated with the unit isotropic stress P and unit shear stresses Q and T. Equation (1) is usually considered without dimensions in order to be applied to holes with different diameters and to materials of diverse elastic properties.

Considering optical techniques, the measured area around the hole is usually expanded, in comparison with strain gages, to an annular region similar to that as shown in Fig 3 (a). The following integral quantities can be defined based on the measurement area of Fig 3 (a) with radius R_1 and R_2 [15] as,

$$\begin{aligned} p &= \frac{1}{aA}\int_0^{2\pi}\int_{R_1}^{R_2} f(r)\, D_r\, r\, dr\, d\theta = \bar{a}\,\frac{1+\upsilon}{E} P \\ q &= \frac{1}{aA}\int_0^{2\pi}\int_{R_1}^{R_2} f(r)\, D_r\, r \cos 2\theta\, dr\, d\theta = \bar{b}\,\frac{1}{E} Q \\ p &= \frac{1}{aA}\int_0^{2\pi}\int_{R_1}^{R_2} f(r)\, D_r\, r \sin 2\theta\, dr\, d\theta = \bar{b}\,\frac{1}{E} T \end{aligned} \tag{3}$$

where

$$\bar{a} = \frac{2\pi}{aA}\int_{R_1}^{R_2} f(r)\,u_r\,r\,dr$$
$$\bar{b} = \frac{2\pi}{aA}\int_{R_1}^{R_2} f(r)\,v_r\,r\,dr \tag{4}$$

and where A is the measurement area and $f(r)$ is a weighting function.

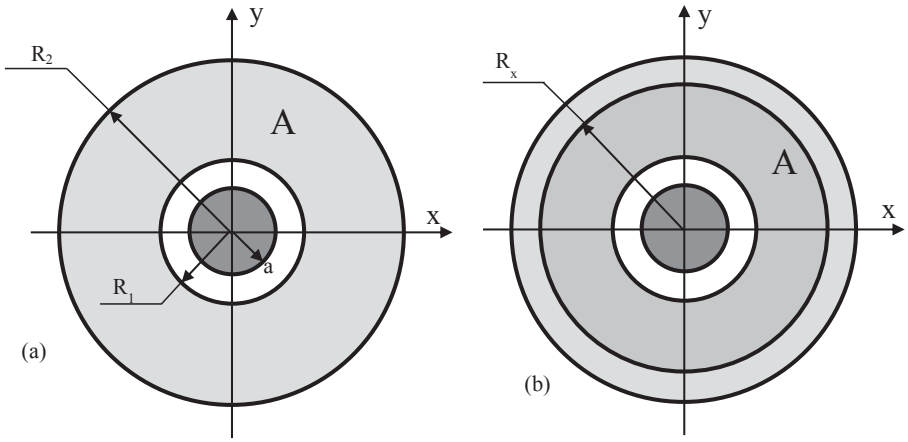

Fig 3. (a) Annular measurement area around the hole. (b) Annular region using weighting functions.

The image data are usually in the form of pixels for practical optical measurements. Integral equations become summation equations in the following way

$$p = \frac{\lambda}{4\pi \sin\psi aN}\sum_i f(r_i)\,\varphi_{ri}$$
$$q = \frac{\lambda}{4\pi \sin\psi aN}\sum_i f(r_i)\,\varphi_{ri}\cos 2\theta_i$$
$$t = \frac{\lambda}{4\pi \sin\psi aN}\sum_i f(r_i)\,\varphi_{ri}\sin 2\theta_i \tag{5}$$

where φ is the phase change at each pixel, and ψ is the sensitivity angle of the interferometer.

Optical measurements usually include displacement artifacts such as generated by rigid body motions or thermal expansion of the camera or the specimen. Theses artifacts can damage the quality of the measurement of displacements and consequently the computed results. Therefore, the residual stress computation process should not be sensitive to them. Considering linear artifacts, Eq (1) expands to [15]

$$\frac{1}{a}D_r(r,\theta) = \frac{1+\upsilon}{E}Pu_r(r) + \frac{1}{E}Qv_r(r)\cos 2\theta + \frac{1}{E}Tv_r(r)\sin 2\theta$$
$$+\frac{1}{a}w_0 + \frac{1}{a}w_x\cos\theta + \frac{1}{a}w_y\sin\theta + \frac{x}{a}s_x\cos\theta + \frac{x}{a}s_y\sin\theta + \frac{y}{a}g_x\cos\theta + \frac{x}{a}g_y\sin\theta \tag{6}$$

where the additional terms respectively refer to a radial shift, an x shift, a y shift, an x stretch, a y stretch, an x shear and a y shear. Thermal expansions produced by the drilling process or by the warm-up of the camera cause x and y stretches. On the other hand, rigid body rotations yield to x and y shears. With these artifacts the p, q, t strains are

$$p = \bar{a}\,\frac{1+\upsilon}{E}P + \frac{2\pi}{aA}\int_{R_1}^{R_2} f(r)\,r\,dr\cdot w_0 + \frac{2\pi}{aA}\int_{R_1}^{R_2} f(r)\,r^2\,dr\cdot\frac{s_x+s_y}{2}$$

$$q = \bar{b}\,\frac{1}{E}\,Q + \frac{\pi}{aA}\int_{R_1}^{R_2} f(r)\,r^2\,D_r \cdot \frac{s_x - s_y}{2}$$
$$t = \bar{b}\,\frac{1}{E}\,T + \frac{\pi}{aA}\int_{R_1}^{R_2} f(r)\,r^2\,D_r \cdot \frac{g_x + g_y}{2} \tag{7}$$

The artifacts presented in Eq (7) can be excluded by selecting the weighting function $f(r)$ such that the associated artifact integral equals to zero. This selection is performed in conjunction with the selection of the processing area by adding a radius R_x to apply this function. (see Fig 3 (b)). Thus

$$\int_{R_1}^{R_2} f(r)\,r\,D_r = 0 \text{ or } \int_{R_1}^{R_2} f(r)\,r^2\,D_r = 0 \tag{8}$$

The previous equations were developed for a single hole drilling step. However, they can be extended to incremental hole drilling where the hole is performed in successive depth increments. In this case, p, q, t and the computed stresses are vectors. Additionally, coefficients $\bar{a}$ and $\bar{b}$ are matrices and they are usually identified in the literature as matrixial coefficients $\hat{\boldsymbol{a}}$ and $\hat{\boldsymbol{b}}$. Reference [15] presented a set of polynomial coefficients to compute these matrices. The coefficients are organized in accordance with the type of interferometer setup (Cartesian or Polar) and with the processing radii used. More details can be found in Ref [15].

2.3 Experimental results

2.3.1 For pipeline samples

Mechanical forming processes are crucial manufacturing steps during the production of pipes employed in petroleum industries for the construction of gas and oil transmission lines. The process consists of applying intense plastic deformation to a steel plate by loading the raw material beyond the yielding point. Thus, considerable residual stress fields are created. They will be able as a favorable or an adverse intrinsic characteristic, of course on dependence of the type and magnitude of the stress. As an example, tensile residual stress fields located at the outer surface of the pipe will be harmful when combined with other stress sources, such as the inner pressure of the transported fluid. This combination could affect the structural integrity of the pipeline and contribute to the premature failure by fatigue, stress corrosion cracking and even fracture [17,18].

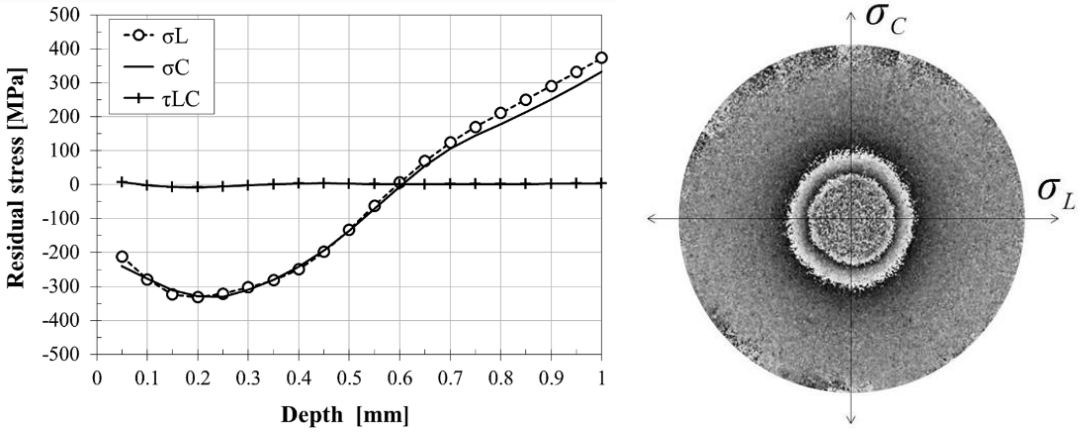

(a) (b)

Fig 4. (a) Typical stress distribution for Pipe 4. (b) Difference phase map for this measurement.

Additionally, buried pipelines are subjected to ground movements and landslides, which may result in plastic deformation, increasing the risk of an accident and sometimes leading to the collapse or

breaking of the transmission line [19]. Therefore, service failures could be produced by the combination of residual stresses and the mechanical stresses caused by predictable (inner pressure) or unpredictable (ground movements) external loads. An evaluation of the residual stress distribution in pipe samples should be performed before the pipe installation to assess the real structural integrity of the final pipeline.

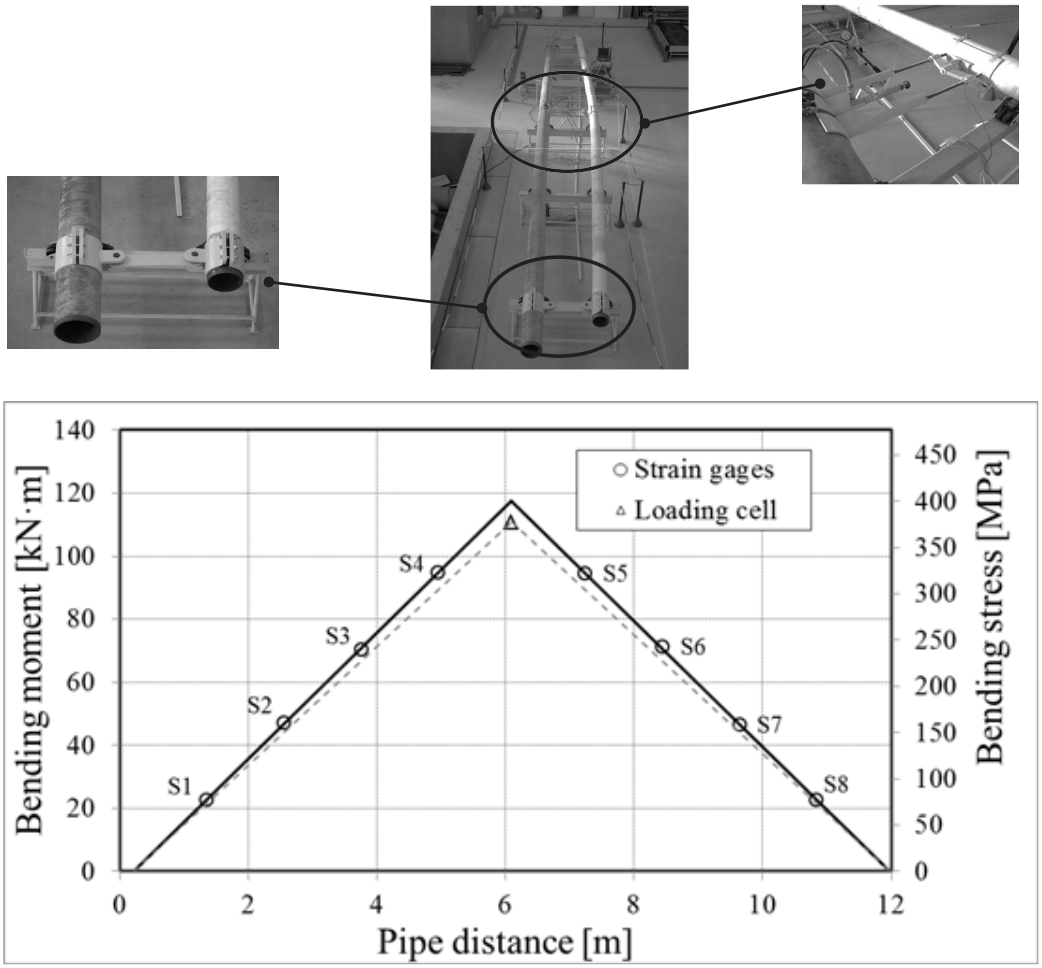

Fig 5. Photographs of the reference bending bench and plot of the obtained bending stress distribution

References 20 and 21 show the experimental residual stress distributions achieved in a set of six pipe samples manufactured with two different processes, namely UOE and ERW. The measurements were performed in both surfaces of the samples (external and internal). As an example, Fig 4 (a) shows a representative stress distribution that was measured in an ERW pipe. The longitudinal (σL) and circumferential (σC) stress distributions are closely matched. Furthermore, the measured shear stress (τLC) is near to zero for all hole increments. Figure 4 (b) shows the phase difference map for the last hole step. The isotropic behavior for the longitudinal and circumferential stresses can be identified from the circular fringes. This behavior was found in most of the measurements, and it indicates that the influence of the manufacturing process on the pipe surface is similar to what should be expected with a shot peening treatment.

2.3.2 For a bending device with pipe samples

An experimental testing bench was designed to estimate the forces applied in buried pipelines under working conditions. Diameter and thickness of pipelines are only defined to withstand the stresses generated by

the internal pressure of the fluid under transportation. Although important, the internal pressure is only one of reasons that contribute to the complex state of stresses acting on pipe walls. Movements associated with the soil are unpredictable loadings. Unfortunately, they can impose unexpected bending and axial loading on pipelines.

Figure 5 shows some photographs of the test bench [22]. The specimens were two pipes 12 m long. A 200 mm nominal diameter pipe, placed on the right of the figure, was used to perform the experiments. The pipe sample placed on the left (external diameter of 250 mm), was used as a complement to apply the bending load. Both pipes were linked by connecting rods (lower inset) to achieve a single supported beam. At the center of the bench, a hydraulic system (upper inset) is used to apply the bending load. A loading cell monitored the load. This setup was used to introduce a well-known bending moment, and a reference bending stress could be computed.

The cross-section of reference pipe was split in eight cross-sections labeled as S1-S8. A couple of strain gauges was installed at diametrically opposite positions to calculate the deformation generated in each cross-section. A maximum load of (29,883±160) N was applied during the experiments.

The non-uniform stress profile along the pipe wall was evaluated in several cross-sections using the hole-drilling method based on the ASTM E837 standard. Each of the evaluated cross-sections was measured at 8 different positions with relative angular spacing of 45°. The data was studied and applied to determine the bending moment and the respective stresses stimulated in the pipe. The measured values were then compared to the reference values calculated previously. Figure 6 (a) shows a photograph taken during a measurement performed in the bench.

A complete procedure for the computation of the bending stresses from DSPI-hole drilling measurements is well detailed in Ref [22]. A summarized version of the procedure is as follows:

(a) *Procedure for an individual hole measurement*: the hole-drilling technique for non-uniform stresses was applied to calculate a set of 20 combined stress values P, Q and T. Additionally, the stresses along the longitudinal and circumferential directions were computed for each step. After that, the twenty measured longitudinal stresses were averaged to obtain a characteristic value, or mean value. This procedure was accomplished for the complete set of holes measured in every cross-section of the pipe.

(b) *Proceeding for an individual cross-section*: the set of eight longitudinal stresses were employed to compute the bending (σ_b) and axial (σ_a) stresses for the cross-section. This procedure was repeated for the eight cross-sections.

(c) *Proceeding for whole set of cross-sections*: bending and axial stresses were plotted along the pipe length. This plot is shown in Fig 5 (b).

2.3.3 Real application case

The hole drilling method and the compact configuration of the radial in-plane interferometer were used outside the laboratory ambient to evaluate combined stresses in a cross-section of a transmission pipeline. The hole drilling measurements were used to determine the bending and axial stress fields generated by the action of the soil around the pipe. After the measurement of residual stress, strain gages were glued in the perimeter of the cross-section of the pipe and the pipeline was cut at a different cross-section. Deformations released by the cutting process were measured by the strain gages and the real effect of the soil on the pipeline was determined. Figure 6 in the far left shows the pipeline section exposed. The center photographs show the interferometer mounted on the pipe. The photograph to the right shows the pipeline after the cut. Figure 7 shows in the right a colored scheme of the cross section with the bending distribution measured by the hole drilling technique (before cutting). In the left, it shows the distribution measured by the strain gages (after cutting). A reasonable agreement between stress magnitudes and bending action can be observed. However, small differences between bending directions were identified. Among the possible sources for this discordance, it can be pointed that the measurements by the hole drilling technique were executed

over a period of two days, and different products were transported in the pipeline, possibly with different inner pressures which could influence the hole drilling measurements as well as the bending computation.

Fig 6. Application example (upper left), optical device (center), pipeline after cutting (bottom right).

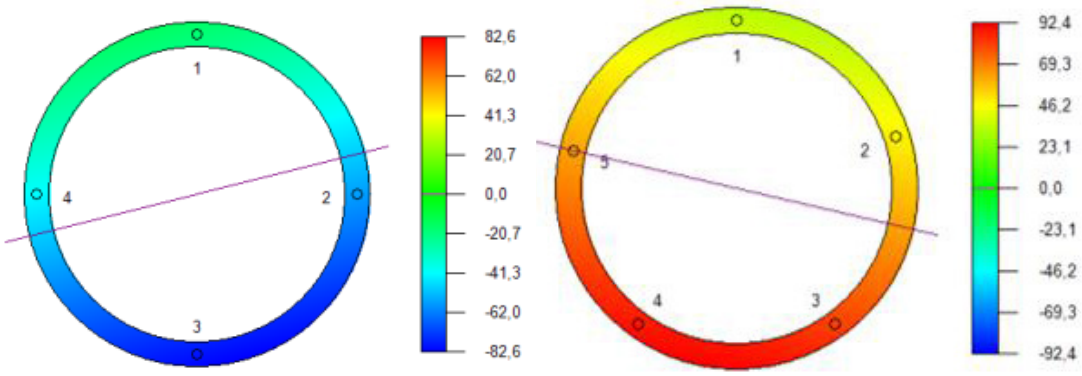

(a) (b)

Fig 7. Bending stress distribution (in MPa) along the measured cross-section. (a) Stresses after cutting (strain gages) and (b) before cutting (with the hole drilling technique).

Finally, it is worth mentioning that the bending stress distributions have opposite signs. They are more compressive for strain gage measurements and more tensile for the hole drilling evaluation. This is expected since strain gages have measured the deformations related to the stresses released by the cutting procedure. On the other hand, the hole drilling computed the stresses acting on the pipe before cutting. Thus, they have similar magnitudes, but opposite signs.

3 Limitations related to the hole depth

3.1 Considerations about the hole depth limitations

The traditional way of measuring the released strains around the hole employs electrical strain gages. After some developments, Rendler and Vigness [4] proposed the design of a standardized strain gage rosette which is used nowadays. The main details of the rosettes are presented in the ASTM E837 standard. Early measurements involved the determination of residuals stress using a uniform stress approach across the whole hole depth. A larger strain response was the most important objective for the rosette design. More modern approaches considered a non-uniform stress distribution along the hole depth [6]. These approaches showed that there was a depth limit to observe the residual stresses. This limit exists because the effect of the released stresses at higher depths becomes ever smaller in the surface due to the Saint Venant principle.

For the Rendler and Vigness rosette setup, the practical limit for the stress depth is achieved at about 1 mm for most commonly nominal size rosettes. Away from that depth, a mathematical singularity in the coefficient matrices used to calculate the stresses impairs the solution and the results become highly unreliable. Because of that, the only way to assess deeper stresses within a material is to use a larger strain gauge rosette and a larger hole diameter [23]. All previous considerations are also valid for optical systems because the hole drilling limitations are related to the stress relief mechanism regardless of the method used to measure the strains/displacements.

As a general case, the stress calculation for the hole drilling technique can be expressed in a matrix form (for strains or displacements) as

$$\bar{\boldsymbol{a}}.\sigma = E.\varepsilon \quad \bar{\boldsymbol{a}}.\sigma = E.\boldsymbol{u_r} \tag{9}$$

Here, ε is the vector of the sequential strains measured after the hole depth steps (for strain gages tests). For interferometric setup u_r, is the vector containing the measured displacements fields. Additionally, σ is the vector containing the computed stresses in each hole depth step and $\bar{\boldsymbol{a}}$ is a matrix of calibration coefficients that relate the stresses to the strains/displacements. Finally, E is the modulus of elasticity. Equation (9) is a shortened form of the complete residual stress computation model, which involves an inverse matrix solution. Readers can find the complete equations for strain gages measurements in the ASTM standard [5]. The complete equations for interferometric setup are detailed in Eqs (1,3,5 and 7). According to these equations, a matrix of coefficients $\bar{\boldsymbol{b}}$ is also needed to produce the complete stress solution.

Figure 8 shows a practical interpretation of the matrix of coefficients $\bar{\boldsymbol{a}}$. Each coefficient a_{ij} in the matrix is related to the deformations released for a unitary stress applied to a depth step j on a hole with i steps. Since the step j is limited to the maximum step number i, i.e., $j \leq i$, the coefficient matrix has a lower triangular form. A more detailed analysis of matrix $\bar{\boldsymbol{a}}$ shows that largest a_{ij} value takes place in the near surface coefficients corresponding to the left side of matrix $\bar{\boldsymbol{a}}$. Conversely, the diagonal and specially the lower right side of matrix $\bar{\boldsymbol{a}}$, which represents steps near the bottom of the hole, has elements of lower magnitudes. The coefficients in the diagonal progressively decrease to a zero value, the matrix turn out to be singular and the computation of the stress is not possible anymore. Reference [23] presents a convenient graphical visualization of the information contained in matrix $\bar{\boldsymbol{a}}$, by using the "cumulative" calibration matrix $\hat{a}$. In this case, each coefficient of matrix $\hat{a}$ is the cumulative sum of the coefficients on the same row of matrix $\bar{\boldsymbol{a}}$. Consequently,

$$\hat{a}_{ij} = \sum_{k=1}^{i} \bar{a}_{ik} \quad \bar{a}_{ij} = \hat{a}_{ij} - \hat{a}_{ij-1} \tag{10}$$

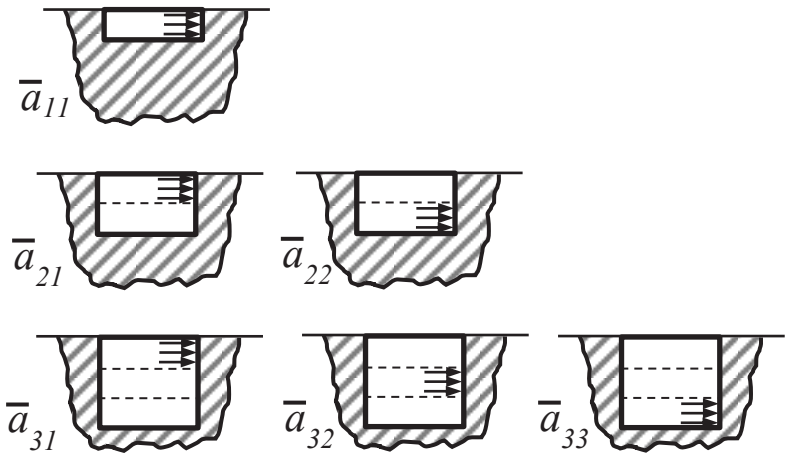

Fig 8. Graphical interpretation of the elements of the coefficient matrix.

As an example, Fig 9 shows contour plots of the cumulative calibration matrices $\hat{\boldsymbol{a}}$ and $\hat{\boldsymbol{b}}$ for a hole of diameter 3 mm. In order to identify the singular point, the matrices were plotted up to a hole depth of 3 mm, considering hole increments of 0.1 mm. If the slope of the contours shown in Fig 9 are analyzed for both matrices, it is possible to identify the singular points. In the case of matrix $\hat{\boldsymbol{a}}$, a likely singular point is reached at a hole depth of approximately 2.3 mm. On the other hand, the diagonal of matrix $\hat{\boldsymbol{b}}$ does not experience the same problem in the range up to 3mm depth. This can be confirmed by analyzing the principal diagonals of matrices $\bar{\boldsymbol{a}}$ and $\bar{\boldsymbol{b}}$ plotted versus the hole depth. Figure 10 shows that the singular point occurs at around 2.3 mm depth (orange point).

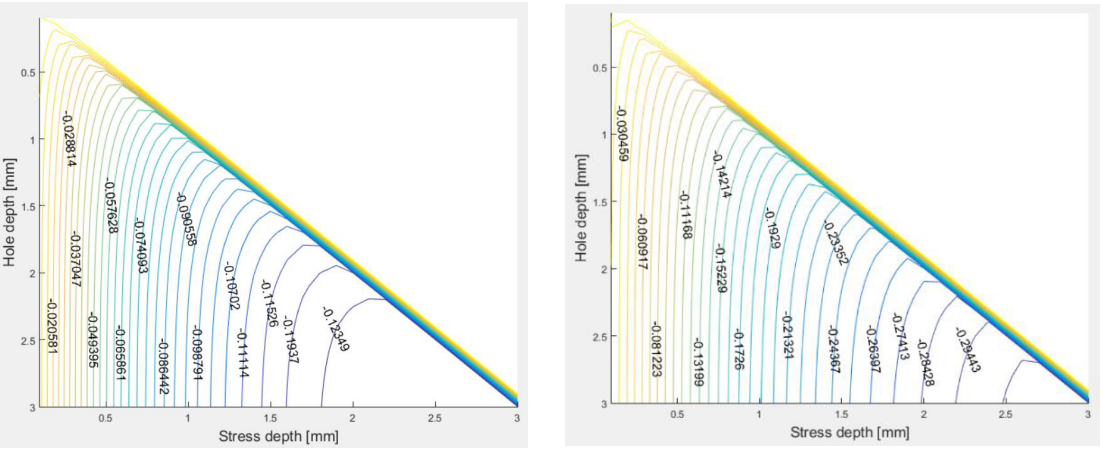

(a) (b)

Fig 9. Graphical interpretation of the elements of the coefficient matrix $\hat{\boldsymbol{a}}$ (left) and $\hat{\boldsymbol{b}}$ (right).

3.2 Alternative approach to increase sensitivity

A modified modular device was designed for drilling larger diameter holes [24], which is an alternative to overcome the limitations concerning the hole depth. The modular configuration involved: (a)

a universal base (UB) which is able to be rigidly clamped to the surface to be measured, (b) a measurement module (MM) that is capable of measuring radial in-plane displacement fields, and (c) a high speed hole-drilling module with manual feed (HDM) that accommodates a larger end mill, up to 3 mm. Figure 11 (a) shows the high speed drill, Fig 11 (b) shows the universal base and Fig 11 (c) shows the measurement module.

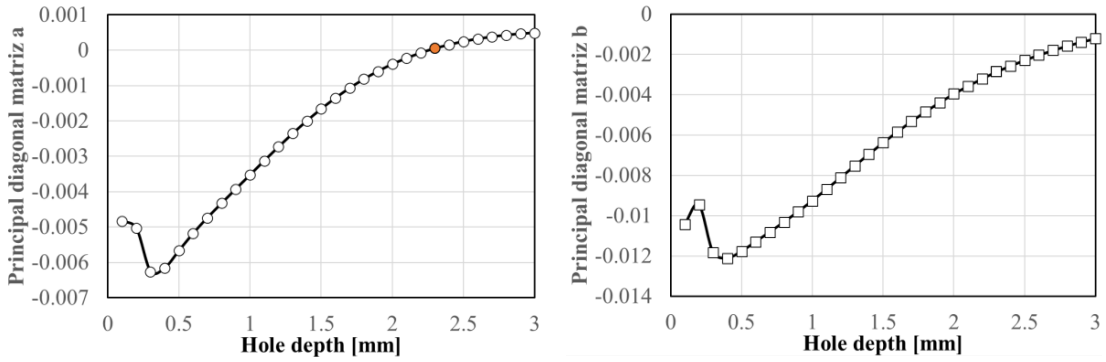

(a) (b)

Fig 10. $\bar{\boldsymbol{a}}$ (left) and $\bar{\boldsymbol{b}}$ (right) diagonal elements along the hole depth for matrices. Hole diameter = 3 mm and hole steps of 0.1 mm.

The MM is similar to the one shown in Fig 1 (b). The hole drilling module is based on a high-speed electrical motor that can run up to 20,000 rpm. The hole depth is controlled by a manual micrometric screw. The measurement and hole-drilling modules are attached to the universal base by using a kinematic interface. As before the repositioning of the modules is quick and accurate. Applying an unloaded specimen, it was validated that the measurement module can be relocated with an error much lower than λ/4. A comprehensive explanation of the kinematic interface can be observed in Ref [24].

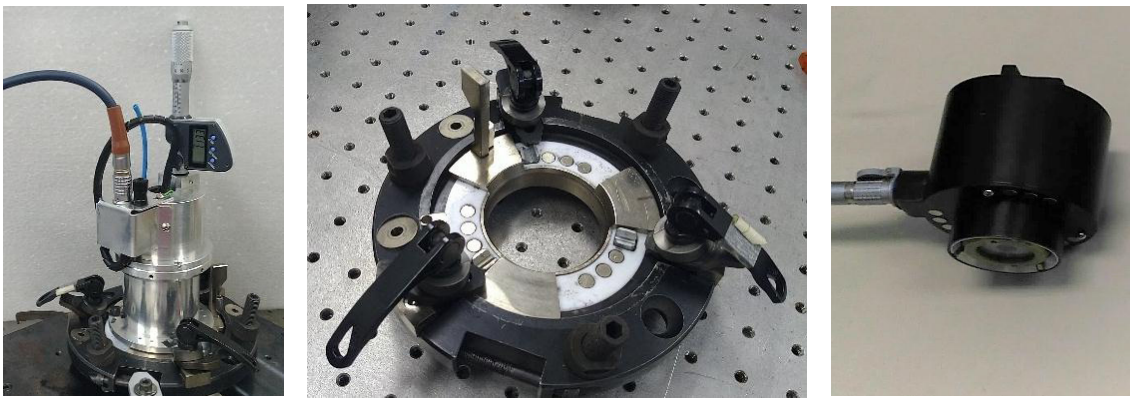

(a) (b) (c)

Fig 11. Photographs of the: (a) hole-drilling module, (b) universal base, and (c) measurement module.

The measurement procedure consists of: (i) - Fixing of the universal base to the surface under measurement. The measurement module is attached to the universal base with kinematic interface. (ii) - Acquire a set of phase-shifted speckle interferograms, calculate the reference phase distribution and store it in the computer memory. (iii) - Replace the measurement module with the hole-drilling module. (iv)- Drill the hole upto the next hole depth increment (v) - After few seconds (for cooling down the measurement region), a second set of phase-shifted speckle interferograms is acquired and a new phase distribution is assessed. (vi)-

A wrapped phase difference map is obtained by subtraction of the post drilling phase map form the reference phase map, and a continuous phase distribution containing the stress relief displacement field is obtained.

3.3 Experimental measurements

Reference 20 details an experimental evaluation of the residual stress distributions in real pipe samples obtained by UOE and ERW processes. The measurements were performed in many cross-sections of long pipe samples (12m in length) and in short ones (0.50 m in length) in which only one cross-section was analyzed. To have a relevant characterization of the stresses, including an average distribution with uncertainty ranges, 8 angular equally spaced points were measured for each cross-section and for the whole set of samples. The results showed that ERW samples have a more well behaved stress profile. For this reason, a short ERW pipe made of API grade X70 steel with an external diameter of 457 mm and a wall thickness of 7.92 mm was selected as a reference residual stress system.

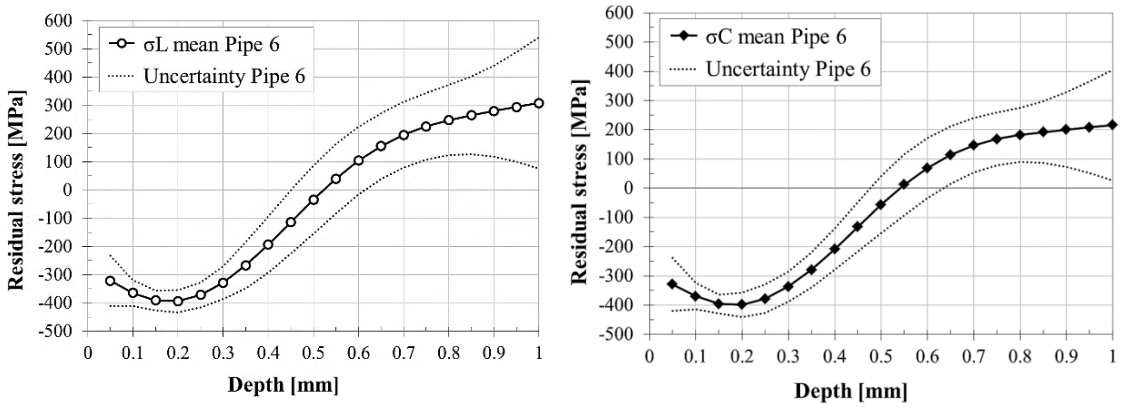

(a) (b)

Fig 12. (a) Mean longitudinal and (b) circumferential stress profiles for the ERW pipe with their respective uncertainty limits.

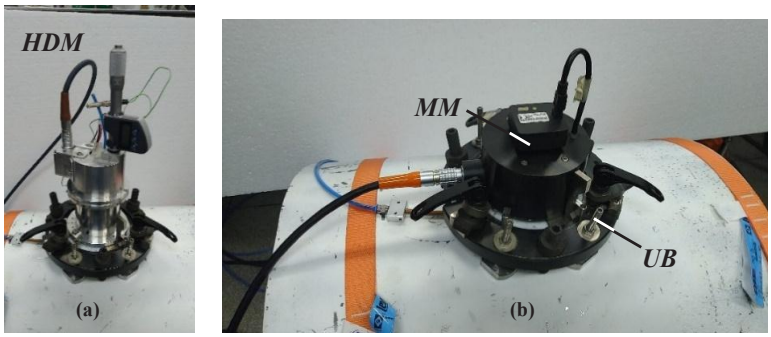

Fig 13. (a) Measurement module. (b) drilling module.

Figures 12 (a) and 12 (b) show the mean longitudinal and circumferential stress profiles determined from a set of 8 measurements measured in the short ERW sample, here named as Pipe 6. Dotted lines represent the upper and lower uncertainty limits for a 95 % confidence interval, calculated by multiplying the corresponding standard deviation of each test step and a t-distribution with 7 degrees of freedom [25].

The sample Pipe 6 was also measured with the device presented in section 3.2. In this case, the hole was drilled with an end mill with 3 mm in diameter. The final depth of 2 mm was achieved in 20 steps of 0.1 mm each. Figure 13 (a) shows the drilling system and the universal base used during the experimental tests. Figure 13 (b) shows the measurement module and universal base during the acquisition step.

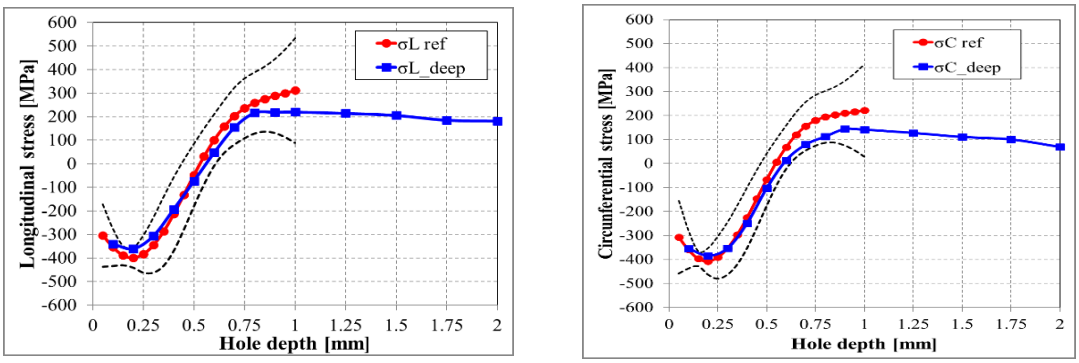

(a) (b)

Fig 14. Longitudinal and circumferential stress distribution .

Figure 14 plots the stress distribution measured up to a hole depth of 2 mm. The measured stress profiles obtained for the larger diameter, deeper hole, agree well with the averaged measurements in Ref 20. Additionally, stress plots are within the uncertainty interval up to a hole depth of 1.0 mm. .

The analysis of the data points shows differences between the averaged results and the new measurements, mainly from 0.8 mm to 1 mm. It is worth mentioning that the reference measurements were executed with a 1.6 mm diameter end mill, and therefore the uncertainty was larger from 0.8 mm onwards. The uncertainty can be explained by the loss of sensitivity during the measurement of the displacement field around the hole. On the other hand, for the newly developed device, the larger hole diameter increases the sensitivity and the results at higher depths are achieved with more confidence.

4 Conclusions

Optical techniques are very attractive for non-destructive testing due to their non-contacting nature, high sensitivity and high relative speed of inspection. The application of digital techniques allows automatic processing and enable systems integration. Additionally, speckle techniques are adequate for the evaluation of real components without further preparation of the surface, which reduce the needs for a skilled operator and is less time consuming.

Speckle techniques can be combined with the hole drilling technique for the determination of residual stresses in mechanical parts used in laboratory rooms or industrial facilities. Compact devices can perform measurements in real applications including the oil and gas industry being an important tool for integrity evaluation. However, some situations require the determination of stresses at higher depths. Usually, for a hole diameter of 1.6 mm, the depth frontier is ~1 mm. To measure stresses at higher depths, large hole diameters should be used. The combination of DSPI with drilling modules using end mills with diameters of 3 mm showed to be a good option to measure deeper stresses. These developments increase the applicability of the hole drilling method to real engineering problems.

References

1. Budynas R G, Nisbett J K, Shigley's Mechanical Engineering Design, 8th edn, (McGraw-Hill Series in Mechanical Engineering), 2006.
2. Samuel A, Weir J, Introduction to Engineering Design, (Elsevier Science & Technology Books), 1999.
3. Lu J, Handbook of Measurement of Residual Stresses, (The Fairmont Press, Lilburn), 1996.
4. Rendler N J, Vigness I, Hole-drilling strain-gage method of measuring residual stresses, *Exp Mech*, 6(1966)577–586.
5. ASTM E837-20, Standard test method for determining residual stresses by the hole-drilling strain-gage method,

Annual Book of ASTM Standards. American Society for Testing and Materials, 2020.

6. Schajer G S, Measurement of non-uniform residual stresses by the hole-drilling method, *J Eng Mater Technol*, 110(1988)338–349.
7. Schajer G S, Hole-drilling residual stress profiling with automated smoothing, *J Eng Mater Technol*, 129(2007)440–445.
8. Wang H P, The alignment error of the hole-drilling method, *Exp Mech*, 19(1979)23–27.
9. Viotti M R, Kaufmann G H, Accuracy and sensitivity of a hole drilling and digital speckle pattern interferometry combined technique to measure residual stresses, *Opt Laser Eng*, 41(2004)297–305.
10. Furgiuele F M, Pagnotta L, Poggialini A, Measuring residual stresses by the hole drilling and coherent optics techniques: a numerical calibration, *J Eng Mater Technol*, 113(1991)41–50.
11. Moore A J, Tyrer J R, An electronic speckle pattern interferometer for complete in-plane measurements, *Meas Sci Technol*, 1(1990)1024–1030.
12. Albertazzi A (Jr), Borges M R, Kanda C, A radial in-plane interferometer for residual stresses measurement using ESPI, Proc SEM IX International Congress on Experimental Mechanics. Bethel: Society for Experimental Mechanics, (2000)108–111.
13. Viotti M R, Albertazzi A(Jr), Kapp W A, Experimental comparison between a portable DSPI device with diffractive optical element and a hole drilling strain gage combined system, *Opt. Lasers Eng*, 46(2008)835–841.
14. Viotti M R, Albertazzi A (Jr), Compact sensor combining digital speckle pattern interferometry and the hole-drilling technique to measure nonuniform residual stress fields, *Opt Eng*, 52 (2013)101905; doi.org/10.1117/1.OE.52.10.101905.
15. Schajer G S, Compact Calibration Data for Hole-Drilling Residual Stress Measurements in Finite-Thickness Specimens, *Exp Mech*, 60(2020)665–678.
16. Viotti M R, Kapp W A, Albertazzi A (Jr), Achromatic digital speckle pattern interferometer with constant radial in-plane sensitivity by using a diffractive optical element, *App Opt*, 48(2009)2275–2281.
17. Law M, Prask H, Luzin V, Gnaeupel-Herold T, Residual stress measurements in coil, linepipe and girth welded pipe, *Mater Sci Eng A*, 437(2006)60–63.
18. Wang J, Saraswat R, Mirzaee-Sisan A, Influence of residual stresses on pipeline integrity: A state-of-the-art review. In: Rio Pipeline Conference & Exposition, Rio de Janeiro, Brazil, (2013), pp 1–10.
19. Zheng J Y, Zhang B J, Liu P F, Wu L L, Failure analysis and safety evaluation of buried pipeline due to deflection of landslide process, *Eng Fail Anal*, 25(2012)156–168.
20. Lothhammer L R, Viotti M R, Veiga C L N, Albertazzi A (Jr), Experimental Evaluation of Residual Stresses in Pipes Manufactured by UOE and ERW Processes, *Exp Mech*, 57(2017)287–296.
21. Lothhammer L R, Viotti M R, Albertazzi A Jr, and Veiga C L N, Residual stress measurements in steel pipes using DSPI and the hole drilling technique, *Int J Press Vessel Pip*, 152(2017)46–55.
22. Pacheco A, Viotti M R, Veiga C L N, Albertazzi A (Jr), Evaluation of Bending Stresses in Pipelines by Using Hole-drilling Measurements Combined with Interferometry, *Exp Mech*, 56(2016)133–143.
23. Schajer G S, Circumferential Rosette Design for Extended Depth Hole-Drilling Residual Stress Measurements, *Exp Mech*, 60(2020)1265–1274.
24. Viotti M R, Albertazzi A (Jr), Bonomo D, Fontana F, Radial in-plane digital speckle pattern interferometer combined with instrumented indentation, *Opt Lasers Eng*, 71(2015)1–8.
25. Montgomery D C, Runger G C, Applied statistics and probability for engineers, 3rd edn, (Wiley, New York), 2003.

[*Received*: 26.05.2022; *revised recd*: 11.06.2022; *accepted*: 15.06.2022]

Matias studied Mechanical Engineering at the Universidad Nacional de Rosario, Argentina. He has been working with optical systems and instrumentation from 2005 in Labmetro, Brazil. He has published more than 30 articles in peer reviewed high IF journals, more than 50 papers in congress proceedings, 1 book (edited by SPIE), 2 Book chapters and 6 Brazilian patents. He was also honoured with the Senior member awards from SPIE (2011) and OSA (2016). His major research interests include: (a) optical techniques for residual stress evaluation as well as nondestructive testing, (b) speckle metrology, (c) digital holography, and (d) digital image processing associated with fringe analysis.

Dr Viotti Matias is Managing Editor (Academics) of Asian J Physics (2022).